

Role of tip shape in light emission from the scanning tunneling microscope

J. Aizpurua* and S. P. Apell

Department of Applied Physics, Chalmers University of Technology and Göteborg University, S-41296 Göteborg, Sweden

R. Berndt

Institut für Experimentelle und Angewandte Physik, Christian-Albrechts-Universität zu Kiel, D-24098 Kiel, Germany

(Received 31 January 2000)

The influence of tip shape on the light produced by scanning tunneling microscopy is analyzed theoretically for the case of noble metals where collective modes enhance the photon emission. We investigate a hyperbolic tip geometry where the aperture of the tip and its apex curvature can be changed independently. The electromagnetic field in the tip-sample region is calculated with the use of the boundary charge method. The tunneling current is treated in a modified Tersoff-Hamann theory. The aperture of the tip is found to control the overall shape of the emission spectrum, while the radius of curvature of the apex is more important for the intensity. Experimentally observed variations of emission spectra may be understood in terms of different tip shapes. The lateral extent of the tip-induced charge density is strongly dependent on the tip shape, and may reach a near-atomic scale for sufficiently sharp tips. This spatial localization has direct implications for the resolution in photonic maps.

I. INTRODUCTION

The scanning tunneling microscope has proven to be a powerful tool to study electronic properties of surfaces on an atomic scale. Photons emitted from scanning tunneling microscopy (STM) yield additional information on local electromagnetic properties.¹⁻⁵ The light emission from metal surfaces in STM is excited by inelastic tunneling of electrons between the tip and sample which couples to localized, collective modes of the tip and the sample (TIP modes).^{6,7} The photon emission has an efficiency of around 10^{-4} photons per tunneling electron.^{6,8,9} This radiative process is mainly governed by two factors: first, the density of states of the tip and the sample determining the tunneling current which serves as an excitation source¹⁰; and second, the electrodynamic properties of the tunneling junction which depend on the materials and the geometry which favors some energies with respect to others.¹¹ In this paper we are concerned with the influence of the shape of the tip on the radiation process. The role of the geometry in STM light emission is important, since the local electromagnetic field distribution governing the emission is sensitive to changes in the boundary conditions of the configuration. In some approximations, the tip was described by means of a sphere^{6,12,13} or a cylinder¹⁴ to mimic the behavior of the tip close to the sample. The gross features in the experimental results can be explained by the use of these geometries, but some deviations found are likely connected with the particular geometries used. Another limitation of existing theories, namely, the neglect of retardation, was recently dealt with by Johansson.¹⁵ Nevertheless, there is room for improvement of the theoretical understanding of a number of experimental observations. In particular, the variability of spectra observed under supposedly similar conditions is likely to be linked to varying tip geometries. This paper therefore aims at an understanding the influence of the tip shape on light emission spectra. Although the exact shape of a tip used in an experiment is usually *unknown*, a theoret-

ical study of tip shape effects may be helpful to establish the role of the tip shape. We note that similar geometrical features are also relevant in other scanning probe microscopy techniques, such as in force measurements using atomic force microscopy, where tip shape plays a crucial role and affects the measured force and force derivative.^{16,17}

As an example of the type of problem we are addressing, in Fig. 1 we show two experimental spectra obtained with different silver tips on a silver sample in ultra-high vacuum. Although the current and bias voltage used in both cases were equal, the spectra exhibit light emission peaks in very different positions. This fact is likely due to the intrinsic characteristics of the tip used, i.e., its particular geometry, as we will show later. Similar effects were also reported for the case of gold tips on gold samples by Péchou *et al.*,¹⁸ who

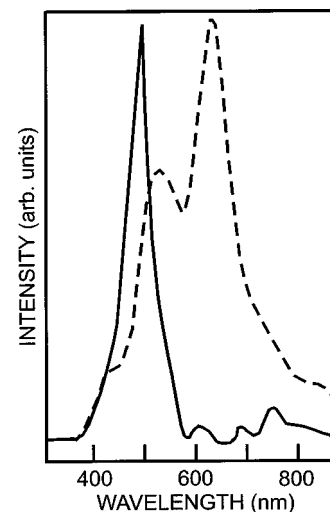


FIG. 1. Experimental light emission spectra for two different silver tips on a silver sample, normalized to the same peak height. The tip bias used in both cases is $V_t = -4$ V. Note the shift in the peak positions.

obtained different spectra of light emission for different tips under the same bias and current conditions, (see Fig. 5 of Ref. 18).

In the framework of a nonrelativistic dielectric theory, properly extended to deal with inhomogeneous situations, it is possible to study what role the shape of a tip has for the spectrum of light emission. In particular, a numerical method based on the boundary charge method,¹⁹ already used for an interpretation of electron energy loss in scanning transmission electron microscopy,^{20,21} allows us to tackle general shapes of both the tip and sample. We calculate the radiated power using a reciprocity theorem which expresses the electromagnetic field at infinity produced by the tunneling current in terms of the local-field enhancement $|G|$ at the junction produced by an external source located at infinity.²² We consider tip shapes which correspond to presumably realistic experimental geometries. In particular, a hyperbolic tip is considered since this geometry allows a control of both the aperture and the curvature of the apex of the tip, separately.²³ The electromagnetic modes of the junction are calculated, since these are important for the spontaneous emission taking place. The coupling of these modes with the inelastic current in terms of radiated power is presented for metallic materials often used in STM configurations such as silver and gold.

II. FORMALISM

A. Radiated power

The total radiated power per unit solid angle Ω and unit photon energy $\hbar\omega$ is⁶

$$\frac{d^2P}{d\Omega d(\hbar\omega)} = 2c\epsilon_0 \sum_{i,f} r^2 |\mathbf{E}_{if}(\mathbf{r}, \omega)|^2 \delta(E_i - E_f - \hbar\omega), \quad (1)$$

where $\mathbf{E}_{if}(\mathbf{r}, \omega)$ is the radiated electric field derived from an electronic transition from the initial state $|i\rangle$ in the tip with energy E_i to the final state $|f\rangle$ in the sample with energy E_f . c is the velocity of light, and $r = |\mathbf{r}|$ is the distance between tip and observer. The electric field at infinity can be expressed by means of the induced field at the cavity with use of a reciprocity theorem²² (see Fig. 2) as

$$\begin{aligned} & \int d^3r' [\delta(\mathbf{r} - \mathbf{r}') \mathbf{j}_o] \cdot \mathbf{E}_{if}(\mathbf{r}, \omega) \\ &= \int d^3r' \mathbf{E}_{ind}(\mathbf{r}, \mathbf{r}', \omega) \cdot \mathbf{j}_{if}(\mathbf{r}', \omega), \end{aligned} \quad (2)$$

where the index (i, f) refers to a particular transition from an initial state $|i\rangle$ to a final state $|f\rangle$. Following the scheme in Fig. 2, $\mathbf{j}_{if}(\mathbf{r}', \omega)$ is the corresponding current density. $\mathbf{E}_{ind}(\mathbf{r}, \mathbf{r}', \omega)$ is the induced field at \mathbf{r}' due to an external current source $\mathbf{j}_o \delta(\mathbf{r} - \mathbf{r}')$ located at \mathbf{r} . They can be related as²²

$$\mathbf{E}_{ind}(\mathbf{r}, \mathbf{r}', \omega) = \frac{i\omega}{4\pi\epsilon_0 c^2} \frac{e^{ikr}}{r} G(\theta, \mathbf{r}', \omega) \mathbf{j}_o, \quad (3)$$

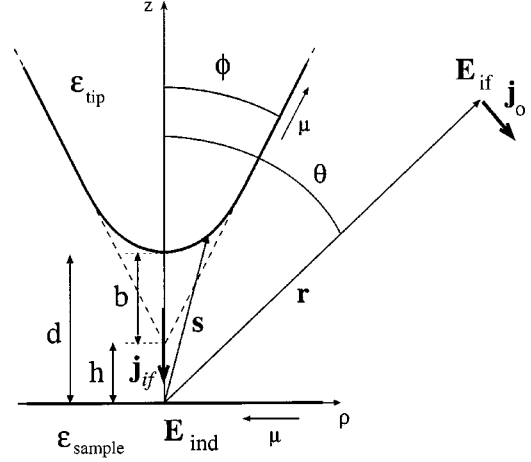


FIG. 2. Geometry for the STM configuration. The aperture of the tip is given by the angle ϕ , and the curvature of the apex is given by the ratio b/d . \mathbf{j}_o , \mathbf{E} , \mathbf{j}_{if} , and \mathbf{E}_{if} denote the sources and fields connected by the reciprocity theorem.

where $G(\theta, \mathbf{r}', \omega)$ represents the local-field enhancement at \mathbf{r}' for a plane wave impinging with angle θ , θ being the angle between \mathbf{r} and the z axis. If we now substitute Eq. (3) into Eq. (2), we obtain

$$\mathbf{E}_{if}(\mathbf{r}, \omega) = \frac{i\omega}{4\pi\epsilon_0 c^2} \int d^3r' G(\theta, \mathbf{r}', \omega) \mathbf{j}_{if}(\mathbf{r}', \omega). \quad (4)$$

The current density gives the electric field at infinity $\mathbf{E}_{if}(\mathbf{r}, \omega)$ when weighted in the integral of Eq. (4) by the local-field enhancement $G(\theta, \mathbf{r}', \omega)$. Therefore, the expression for the radiated power becomes

$$\begin{aligned} \frac{d^2P}{d\Omega d(\hbar\omega)} &= \frac{\omega^2}{8\pi^2\epsilon_0 c^3} \sum_{i,f} \left| \int d^3r' G(\theta, \mathbf{r}', \omega) \mathbf{j}_{if}(\mathbf{r}', \omega) \right|^2 \\ &\times \delta(E_i - E_f - \hbar\omega). \end{aligned} \quad (5)$$

In this expression two main factors determine the radiated power: the current density \mathbf{j}_{if} and the local-field enhancement G .

B. Current density

The current density $\mathbf{j}_{if}(\mathbf{r}', \omega)$ can be expressed in terms of the transition from the tip state $|i\rangle$ to the sample state $|f\rangle$. Within the transfer Hamiltonian approach,²⁴⁻²⁶

$$\begin{aligned} \hat{z} \cdot \mathbf{j}_{if}(\mathbf{r}', \omega) &= \frac{e}{i\hbar} \left[\frac{\hbar^2}{2m} \left(\frac{\partial \psi_f^*}{\partial z'} \psi_i - \psi_f^* \frac{\partial \psi_i}{\partial z'} \right) (\mathbf{r}') \right. \\ &\left. + E_{fi} \int_0^d dz \Theta(z' - z) \psi_f^* \psi_i(\mathbf{r}) \right], \end{aligned} \quad (6)$$

where ψ_i and ψ_f account for the left- and right-hand-side wave functions which describe the tunneling process in the junction. The tip-sample separation distance is d , and \hat{z} is the unit vector perpendicular to the sample surface. $E_{fi} \equiv E_f - E_i = -\hbar\omega$ is the energy difference between the initial and final states, and $\Theta(x)$ is the Heaviside step function, which

takes into account the fact that the inelastic process occurs at a particular point in the cavity z' . Indeed, the last term on the right-hand side of Eq. (6) accounts for tunneling transitions in which the energies of the states involved are not equal.

We perform the integration over the current density in the transverse direction, and define

$$M_{fi}(z_o, \omega) \equiv \int d^2\mathbf{S}' \cdot \left[\frac{\hbar^2}{2m} \left(\frac{\partial \psi_f^*}{\partial z'} \psi_i - \psi_f^* \frac{\partial \psi_i}{\partial z'} \right) (\mathbf{r}') \right]_{z'=z_o} - \hbar \omega \int_0^d dz \Theta(z_o - z) \psi_f^* \psi_i(\mathbf{r}). \quad (7)$$

The local-field enhancement factor can be taken out of the integral in the transverse direction in Eq. (5), since its decay in this direction is slower (algebraic) than the decay of the current given by the exponential decay of the tip wave function itself. The radiated power can then be expressed as

$$\begin{aligned} \frac{d^2P}{d\Omega d(\hbar\omega)} &= \frac{\alpha}{h} \left(\frac{\omega}{c} \right)^2 \\ &\times \sum_{i,f} \left| \int dz_o M_{fi}(z_o, \omega) G(\theta, z_o, \omega) \right|^2 \\ &\times \delta(E_i - E_f - \hbar\omega), \end{aligned} \quad (8)$$

where α is the fine-structure constant.

The matrix element $M_{fi}(z_o, \omega)$ can be directly related to a current $I(z_o, \omega)$ (Ref. 25) for a certain bias V_t :

$$\begin{aligned} I(z_o, \omega) &= \frac{4\pi e}{\hbar} \sum_{i,f} [f(E_i - eV_t) - f(E_f)] |M_{fi}(z_o, \omega)|^2 \\ &\times \delta(E_i - E_f - \hbar\omega). \end{aligned} \quad (9)$$

We use Tersoff and Haman's theory²⁶ to describe the tunneling current and extend this theory to include large bias voltages.²⁷ This theory includes the radius of curvature of the tip in the description of the current by means of a parameter R in the wave function describing the tip,

$$\psi_t = \psi_i = \Omega_t^{-1/2} C_t \kappa_i R e^{\kappa_i R} (\kappa_i |\mathbf{r} - \mathbf{r}_o|)^{-1} e^{-\kappa_i |\mathbf{r} - \mathbf{r}_o|}, \quad (10)$$

with \mathbf{r}_o the position of the center of curvature, and

$$\kappa_i = \sqrt{\frac{2m}{\hbar^2} (E_F^t + \phi^t - E_i)} \quad (11)$$

the inverse decay length of the tip wave function given by the Fermi energy of the tip E_F^t and the tip work function ϕ^t . E_i is the energy of the initial states at the tip, C_t is a normalization constant or order unity,²⁶ and Ω_t is the volume of the tip.

We adopt WKB solutions in the z direction to account for the change in the value of the potential barrier at the tunneling junction. The inverse decay lengths of the tip and sample depend on the z coordinate in such a way that the potential in the cavity is the same for both of them at a given point,

$$\kappa_{f(i)}(z) = \sqrt{\frac{2m}{\hbar^2} \left(E_F^s + \phi^s + (eV_t + \phi^t - \phi^s) \left[\frac{d-z}{d} \right] - E_{f(i)} \right)}, \quad (12)$$

which depends on the Fermi energy of the sample E_F^s , the work functions ϕ^s and ϕ^t and the applied bias V_t . $E_{f(i)}$ is the energy of the final (initial) state and $z=0$ corresponds to the position at the tip (initial state).

In the WKB approximation the sample wave function is given by

$$\psi_s = \psi_f = \Omega_s^{-1/2} C_s e^{i\mathbf{k}_\parallel \cdot \boldsymbol{\rho}} \sqrt{\frac{\kappa_f^*(z=d)}{\kappa_f^*(z)}} e^{-\int_z^d \kappa_f^*(z') dz'}, \quad (13)$$

where $\boldsymbol{\rho}$ is the coordinate along the transverse direction,

$$C_s = \frac{2ik_\perp}{ik_\perp - \kappa_f(z=d)}$$

is a normalization constant. k_\perp and k_\parallel are the perpendicular and parallel components of the momentum of the final state respectively, and $\kappa_f^*(z) = \sqrt{\kappa_f^2(z) + k_\parallel^2}$.

If we assume a free-electron gas to describe both tip and sample materials, the matrix element connecting the initial and final states in Eq. (7) becomes

$$\begin{aligned} M_{fi}(z_o, \omega) &= (\Omega_s \Omega_t)^{-1/2} \frac{2ik_\perp}{ik_\perp - \kappa_f} 2\pi R \sqrt{\frac{\kappa_f^*(z_o)}{\kappa_i^*(z_o)}} e^{(\kappa_i - \kappa_f^*)R} T_{fi}(z_o, \omega), \\ & \quad (14) \end{aligned}$$

with $\kappa_i = \kappa_i(z=0)$, $\kappa_f = \kappa_f(z=d)$, and

$$\begin{aligned} T_{fi}(z_o, \omega) &= \frac{\hbar^2}{2m} \\ &\times \frac{\left\{ \left(\frac{\kappa_i^*(z_o)}{2\kappa_i^*(z_o)} - \frac{\kappa_f^*(z_o)}{2\kappa_f^*(z_o)} - \kappa_i^*(z_o) - \kappa_f^*(z_o) \right) \right\}}{\sqrt{\kappa_i^*(z_o) \kappa_f^*(z_o)}} \\ &\times e^{-\int_0^{z_o} \kappa_i^*(z') dz'} e^{-\int_{z_o}^d \kappa_f^*(z') dz'} \\ &- \hbar \omega \int_{z_o}^d dz \frac{e^{-\int_0^z \kappa_i^*(z') dz'} e^{-\int_z^d \kappa_f^*(z') dz'}}{\sqrt{\kappa_i^*(z) \kappa_f^*(z)}}, \end{aligned} \quad (15)$$

Now, in order to calculate the tunneling current, we turn the sum over initial and final states (i, f) into a sum over momentum components:

$$\begin{aligned}
I(z_o, \omega) &= \frac{em}{\pi \hbar^3} R^2 \int_{\max\{0, E_F^s - E_{\parallel}\}}^{E_F^s + eV_t - \hbar\omega - E_{\parallel}} dE_{\perp} \int_o^{E_F^s + eV_t - \hbar\omega} \\
&\times dE_{\parallel} \frac{\kappa_f^*}{\kappa_i^*} e^{2(\kappa_i - \kappa_i^*)R} \frac{(E_{\perp})^{1/2} (E_{\parallel} + E_{\perp} + \hbar\omega)^{1/2}}{\left(E_{\perp} + \frac{\hbar^2}{2m} \kappa_f^2\right)} \\
&\times \left[\frac{2m}{\hbar^2} T_{fi}(z_o, \omega) \right]^2. \tag{16}
\end{aligned}$$

The distance between the tip and sample d is fixed by the elastic current $I_{\text{elas}} = I(\omega = 0)$ at a given tip bias V_t . Typically, d is in the range of 4–7 Å for elastic currents from 200 nA down to 5 nA.

C. Local-field enhancement: boundary charge method

In order to study of the local field enhancement $G(\theta, z, \omega)$, we use the boundary charge method^{19–21} to calculate the electromagnetic field distribution for a realistic shape of the tip. This method consists of solving Poisson's equation by means of a surface integral involving the surface charge density $\sigma(\mathbf{s}, \omega)$ induced at the interfaces separating two different media. The field \mathbf{E}_{ind} (see Fig. 2) from a unit current source $\mathbf{j}_o \delta(\mathbf{r} - \mathbf{r}')$ at infinity can be found, therefore, by means of the surface charge density originated by this particular source. The self-consistent integral equation for the surface charge density is^{20,21}

$$\Lambda \sigma(\mathbf{s}, \omega) = -\mathbf{n}_s \cdot \nabla \phi^{\text{ext}}(\mathbf{s}, \omega) - \int \frac{\mathbf{n}_s \cdot (\mathbf{s} - \mathbf{s}')}{|\mathbf{s} - \mathbf{s}'|^3} \sigma(\mathbf{s}', \omega) d\mathbf{s}', \tag{17}$$

where the vector positions \mathbf{s} and \mathbf{s}' refer to interface points in Fig. 2, \mathbf{n}_s is the unit vector normal to the interface at point \mathbf{s} , and $-\nabla \phi^{\text{ext}}(\mathbf{s}, \omega)$ is the ω component of the external field acting at \mathbf{s} , due to a source at infinity.

$$\Lambda = 2\pi \frac{\varepsilon_2(\omega) + \varepsilon_1(\omega)}{\varepsilon_2(\omega) - \varepsilon_1(\omega)} \tag{18}$$

depends on the ratio of the two dielectric functions ε_1 and ε_2 surrounding each interface point \mathbf{s} , to the left and right of the direction of the parametrization (μ), respectively.

Assuming rotational invariance, Eq. (17) can be properly projected by means of an expansion in the azimuthal angle φ ,

$$\sigma(\mathbf{s}, \omega) = \frac{1}{2\pi} \sum_m \sigma_m(\mu, \omega) e^{im\varphi}, \tag{19}$$

where μ is a parameter running along the interfaces in the ρ - z plane. This expansion makes it possible to characterize Eq. (17) by the conserved azimuthal number m ,

$$\Lambda(\omega) \sigma_m(\mu, \omega) = f_m(\mu, \omega) + \int d\mu' F_m(\mu, \mu') \sigma_m(\mu', \omega), \tag{20}$$

where $F_m(\mu, \mu')$ are the interaction matrix elements which connect the points μ and μ' . This interaction matrix connecting the different points only depends on the geometrical

features of the system. Its explicit expression in terms of a parametrization $[\rho_s(\mu), z_s(\mu)]$ is

$$\begin{aligned}
F_m(\mu, \mu') &= \rho_s(\mu') \sqrt{\rho_s'(\mu')^2 + z_s'(\mu')^2} \\
&\times \int d\varphi \frac{A - C \cos \varphi}{(B - D \cos \varphi)^{3/2}} e^{im\varphi}, \tag{21}
\end{aligned}$$

where the primes denote the derivative with respect to the parameter μ , and

$$A = n_{\rho} \rho_s(\mu) - n_z [z_s(\mu) - z_s(\mu')],$$

$$B = \rho_s^2(\mu) + \rho_s^2(\mu') + [z_s(\mu) - z_s(\mu')]^2,$$

$$C = n_{\rho} \rho_s(\mu'),$$

$$D = 2\rho_s(\mu) \rho_s(\mu').$$

$(n_{\rho}, n_z) = (z_s'(\mu), -\rho_s'(\mu)) / \sqrt{\rho_s'(\mu)^2 + z_s'(\mu)^2}$ stands for the radial and z components of the interface normal, and $f_m(\mu, \omega)$ is the projected external field produced by the current source located at infinity. In our case, we assume a hyperbolic parametrization to describe the tip as shown in Fig. 2, where it is possible to control both the curvature (by means of the distance b versus tip-sample distance $d = b + h$) and the aperture (by means of the aperture angle ϕ) of the tip. The explicit parametrization for this case is:

$$\rho(\mu) = b \tan(\phi) \sinh(\mu),$$

$$z(\mu) = h + b \cosh(\mu),$$

where the shortest distance between tip and sample is $d = h + b$. The radius R included in Eq. (16) can be related to the curvature radius of the tip at the symmetry point as

$$R = \frac{(\rho'(\mu)^2 + z'(\mu)^2)^{3/2}}{\rho''(\mu)z'(\mu) - \rho'(\mu)z''(\mu)} \Big|_{(\mu=0)} = b \tan^2(\phi), \tag{22}$$

which is the main reason for the strong dependence of the tunneling current $I \propto R^2$ on the curvature and aperture of the tip.

Once the surface charge distribution is obtained along the two interfaces (hyperbole and plane), the local-field enhancement G is obtained straightforwardly as

$$G(\mathbf{r}, \omega) = \frac{\hat{z} \cdot [\nabla \phi^{\text{ext}}(\mathbf{r}, \omega) + \nabla \phi^{\text{ind}}(\mathbf{r}, \omega)]}{\hat{z} \cdot [\nabla \phi^{\text{ext}}(\mathbf{r}, \omega)]}, \tag{23}$$

where the induced part is given by the surface charge density calculated in the framework of the boundary charge method:

$$\nabla \phi^{\text{ind}}(\mathbf{r}, \omega) = \int \frac{(\mathbf{r} - \mathbf{s}')}{|\mathbf{r} - \mathbf{s}'|^3} \sigma(\mathbf{s}', \omega) d\mathbf{s}' \tag{24}$$

This equation is a key element which takes into account the different boundaries corresponding to the geometrical shapes at hand. In Sec. III, we use it to calculate mode energies of the cavity.

III. MODES OF THE CAVITY

Before continuing to calculate the modes and the photon spectra it is worthwhile to have a closer look at the relation between geometry and mode energies. These modes determine the most probable energies for the inelastic tunneling electrons to decay into photons. They are strictly governed by the geometry of the junction. For simplicity, we characterize both the tip and sample as metals with a plasma frequency ω_p . In Fig. 3 we show the surface charge density associated with the lowest-energy collective modes of a metallic tip and sample for three different cases. Figure 3(a) corresponds to a sharp tip whose aperture angle $\phi=20^\circ$. The surface charge density is extremely localized. We find a spatial extension of the induced surface charge of merely 2 nm (a tip-sample separation $d=5 \text{ \AA}$). At the same separation, for a more open tip with an aperture angle $\phi=70^\circ$ [Fig. 3(b)], the energy of the mode is slightly shifted upward. More importantly, the spatial extent of the surface charge density around the junction becomes much wider. In this case, the mode spreads out up to 15 nm, which is one order of magnitude larger than in the previous case. A model based on a sphere-plane system to model the junction resembles more the behavior of the open tip, as can be seen in Fig. 3(c) for a 300- \AA radius sphere over a plane at the same separation of 5 \AA . The large coupling area allows the surface charge density of the lowest mode to spread even further than in the case of an open hyperbolic tip. The low energy of this mode is connected with the large coupling between surfaces in the case of both the open hyperbolic tip and the spherical tip, and with the larger coupling within the tip itself in the case of the sharp tip, which confines the surface charge density to the apex. In all the cases, the lowest mode shows an approximately dipolar pattern.

The lateral extent of this lowest mode has implications for the spatial resolution of light emission maps. Depending on the shape of the tip, the light emission peaks are related to larger (open tip) or smaller (sharp tip) areas on the sample close to the junction, yielding a different resolution power. It may be that the unexpected localization to a near-atomic scale has already been observed in experiments, where atomic resolution in photon mapping was achieved.²⁸ To model the observed lateral extent of intensity variations in those experiments, a lateral extent of the TIP mode of ≈ 2 nm had to be assumed. This value is surprisingly similar to what we find for a sharp tip.

The complete set of eigenfunctions found from Eq. (17) for a hyperbolic tip next to a planar surface with no external source is shown in Fig. 4 for various cavities (b/d , ϕ). Only modes with $m=0$ are plotted, since these are the only ones being excited by the current at the symmetry axis (rotational invariance). In Fig. 4(a), the spectrum of modes for the case of a hyperboloid-plane system is shown as a function of the dimensionless parameter b/d characterizing the curvature of the tip apex (cf. Fig. 2). The aperture angle ϕ is maintained equal to 30° . The mode positions are expressed in units of the square of the plasma frequency ω_p . In this case the modes are shifted down in energy when compared with modes belonging to other geometries, such as the sphere-plane case.⁶ As pointed out above, this is due to a larger localization of the surface charge density associated with the

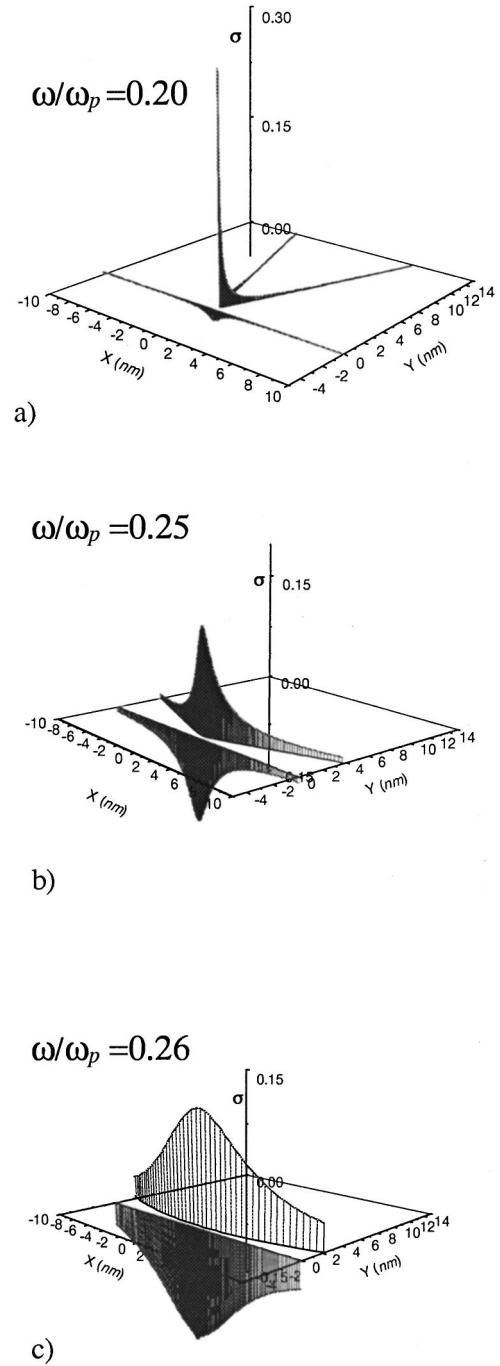


FIG. 3. Surface charge density σ of the lowest-order mode for three different junctions. (a) Hyperbolic tip of 20 degree aperture. Hyperbolic tips of the 70° aperture (b) and the 300- \AA spherical tip (c). In all cases the parameter characterizing the apex has been fixed to $b/d=2/3$, with a tip-sample distance $d=5 \text{ \AA}$. Note the different spatial localization of the induced charge density.

modes, close to the end of the tip. For typical tunneling distances of around 5 \AA , the difference in the mode positions can exceed $0.1\omega_p$, which can be of the order of tenths of eV in real situations. As we increase the curvature of the tip apex (by increasing the value of b/d), there is a tendency for the modes to shift upward, but this tendency is slow and does not noticeably change the value of the resonances. In Fig. 4(b) we show the dependence of the modes as a function of the aperture of the tip (ϕ) for a fixed value of $b/d=2/3$

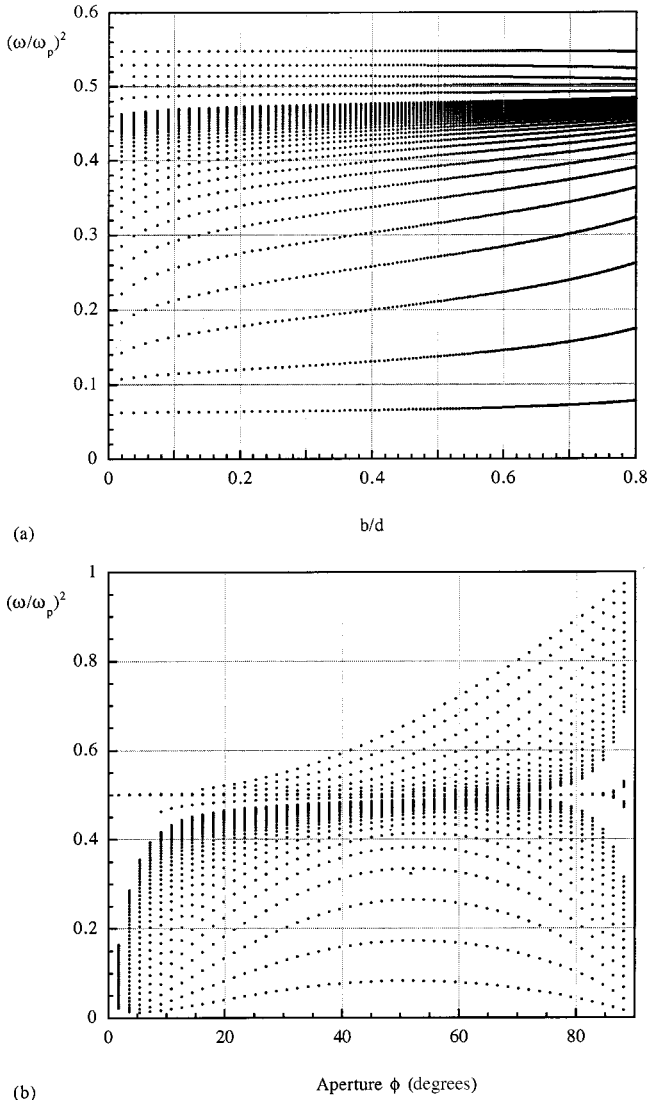


FIG. 4. (a) Modes of a STM cavity as a function of the ratio b/d characterizing the curvature of the tip apex for a fixed aperture of $\phi=30^\circ$. (b) Modes of a STM cavity as a function of the aperture of the tip (ϕ) for a fixed value of $b/d=2/3$. In both cases tip and sample are characterized by means of a plasma frequency ω_p , and only modes with $m=0$ are shown (full azimuthal symmetry). The mode positions change more noticeably when changing the aperture rather than the apex curvature.

characterizing the curvature. As the aperture of the tip becomes more narrow ($\phi \rightarrow 0^\circ$), the modes are shifted downward in energy because of a more localized collective resonance at the tip. For larger apertures ($\phi \rightarrow 90^\circ$), the modes are again shifted downward but also upward depending on the nature of the surface charge density associated with the modes. As a consequence of a larger area of interaction between tip and sample, which resembles the behavior of a cavity formed by two parallel interfaces, there exist symmetric and antisymmetric modes which correspond to mode positions larger or smaller than the planar resonance at $\omega_p/\sqrt{2}$, respectively. This is also the mechanism which generates low-energy modes in the case of a sphere-sample system. In the intermediate region, where $\phi \approx 45^\circ$, each mode with $\omega^2 < 1/2$ assumes its largest energy.

Generally, one can conclude that the effect of the aperture

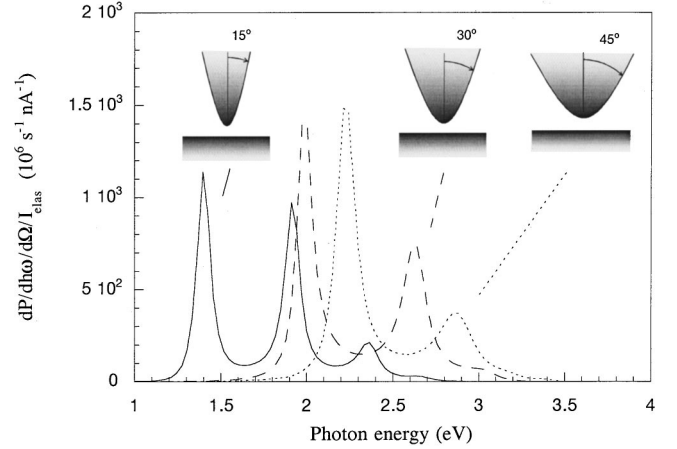


FIG. 5. Comparison between light-emission spectra for the case of an Ag tip and an Ag sample for different apertures of the tip ($\phi=15^\circ$, 30° , and 45° in solid, dashed, and dotted lines, respectively). The tip-sample distance is fixed at 5 \AA , and the bias is 4 V . The peaks have been normalized by the elastic current corresponding to each case in order to improve the validity of the comparison ($b/d=2/3$ in all cases). Peak positions are strong functions of the aperture angle, but the intensity is similar after normalization, with a slight tendency to increase for more open tips.

on the spectrum of cavity modes is more pronounced than the effect of the sharpness at the apex. Thus minor details of the tip apex do not influence the position of the resonances as strongly. Going beyond a free-electron model, we note, however, that the tip apex has a drastic influence on the tip density of states.¹⁰ For this reason, the spectral features may still depend on the tip apex even though the electromagnetic modes remain unaffected.

IV. LIGHT EMISSION

We now show the main differences in the radiated power arising for different tip geometries of interest. We extend the well-known case of the sphere-plane system⁶ to the hyperboloid plane, and study the effect of the sharpness and curvature of the tip in the light emission spectrum. In order to make a systematic study of the aperture on the one hand and on the curvature of the apex on the other hand, we first fix the tip-sample distance and change both parameters separately. Later, we study the case of a constant current, i.e., varying the separation distance d to obtain the same elastic current in all cases, which is more typical of experimental procedures.

A. Effect of the sharpness

Different apertures (ϕ) of the tip cone strongly influence the position of the cavity resonances, as shown in Fig. 4(b); therefore, one should expect a change in the radiation peak positions as the aperture of the tip is modified. We first study the case of a silver tip on a silver sample, since it is a system which shows well-defined peaks in experiments.⁷ We take a value of $b/d=2/3$ characterizing the curvature of the apex of the tip, and change the aperture of the hyperbolic tip from 15° up to 45° , as shown in the insets of Fig. 5. The peak positions of the light emission follow the tendency described

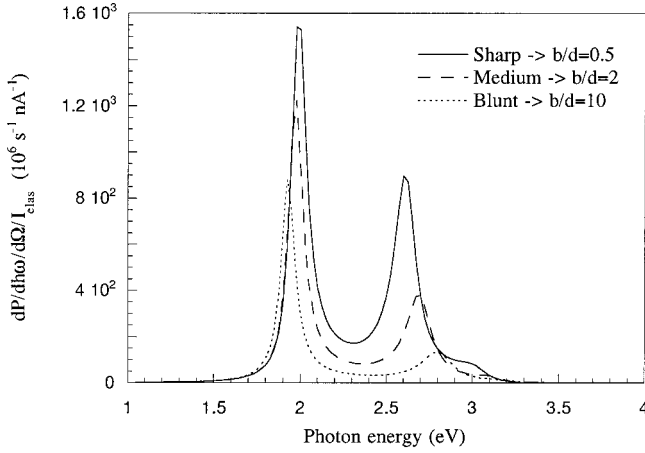


FIG. 6. Radiated power for three different silver tips on silver samples normalized to the elastic tunneling current. The parameters used to characterize the tips are shown in the inset ($b = 2.5, 10$, and 50 \AA , respectively), the aperture ϕ is fixed to 30° and the distance between the tip and sample is 5 \AA . The bias applied is 4 V . In contrast to Fig. 5, we now see how the apex controls the intensity rather than the peak positions.

in Sec. III: as the aperture ϕ increases up to 45° , the low-energy peak is shifted upward (from 1.4 to 2.3 eV), and slightly downward again to 2.2 eV when the aperture increases beyond 45° . Comparing to the experimental observations of Fig. 1, we suggest that tips with different apertures may have been involved in this experiment.

As to the intensity of the field enhancement, we find a clear tendency for the absolute strength to increase as the aperture becomes larger. This tendency is due to the fact that the effective tunneling area grows and strongly increases the elastic current I_{elas} . In Fig. 5 the radiated power per unit energy and unit solid angle is plotted for the three apertures shown in the insets. The strength of the curves is divided by the elastic tunneling current calculated in the same way, in order to make a more proper comparison. The field enhancement $|G|$ at the junction is also increasing for a given bias and distance when the aperture becomes larger due to a larger interaction area between the two interfaces. This tendency is less dramatic than the tendency for the current to increase. This is the reason why all intensities are comparable after normalization.

B. Effect of the apex curvature

The curvature of the extreme part of the tip is a feature that can be controlled in our formalism by means of the parameter b/d , which describes the fine details of the STM junction. The variation of the resonances as a function of this parameter has been found to be less drastic, as the tendency of the modes showed. As an example, in Fig. 6 we show the spectrum of light emission for a silver tip and a silver sample when the separation d is fixed to 5 \AA , for a bias of 4 V . The different spectra have been normalized to their corresponding elastic currents. The sharpness of the tip increases when b changes from $b = 50 \text{ \AA}$ to $b = 2.5 \text{ \AA}$ and, maintaining the aperture ϕ fixed to 30° , the positions of the main peaks remain constant, and only a slight variation in the high-energy peak position is observed. The change in the peak

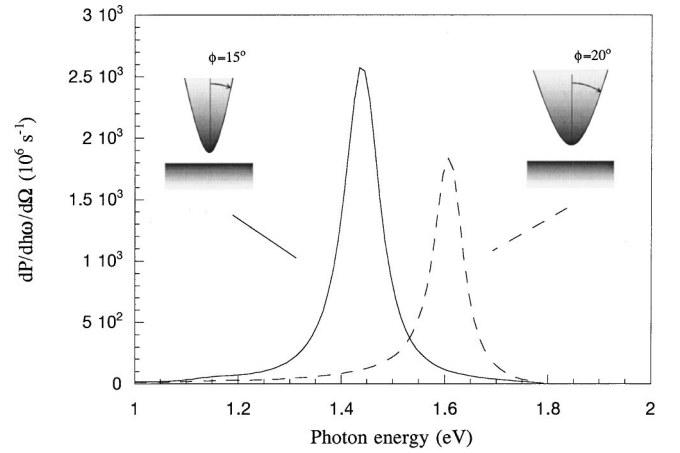


FIG. 7. Comparison between light emission spectra for the case of a Au tip and Au sample for different apertures of the tip ($\phi = 15^\circ$ and 20°) with $d = 4.3$ and 4.75 \AA . The tip-sample distance is fixed in order to obtain an elastic current of 15 nA for a bias of 1.8 V . Note that a slight change in the aperture clearly modifies the position of the emission peaks, while the intensity remains fairly constant.

position of the radiated power is negligible when compared with the change originating from modifications of the aperture angle under the same conditions of bias and current, as we described in Sec. III. The absolute intensity of the peaks increases, however, as the tip becomes more blunt (greater values of b). Again, the effective area of tunneling is causing this increase, although the field enhancement is larger for sharper tips, as shown in the normalized figure.

C. Effect of the tip-sample distance

In the previous sections we have fixed the tunneling distance in order to isolate the role of the aperture and curvature from any other influence in the spectrum of light emission. In practice, the quantity usually controlled is the total tunneling current I_{elas} .

The total current for a given bias can be controlled by means of the tip-sample separation. As discussed for the case of constant distance, the mode positions are going to be governed mainly by the aperture ϕ . More details are found when studying the intensity of peaks in the spectrum, as we change the sharpness or curvature of the apex while maintaining the same tunneling current. When the aperture of the tip becomes larger, more extended portions of the tip and sample interfaces are closer, giving rise to a larger tunneling current. This fact also causes a larger field enhancement due to a more effective coupling of the two interfaces. Now, in order to work in a constant-current mode, we are forced to spatially separate the tip and sample to keep the same current. This decreases the field enhancement as a consequence of the weaker interactions between the interfaces. These opposite tendencies cancel to some extent depending on the particular material and cavity. In Fig. 7, the radiated power per unit energy and unit solid angle is shown for the case of a Au tip and Au sample for two different apertures of the tip ($\phi = 15^\circ$ and 20° , respectively). The distances between the tip and sample are 4.3 and 4.75 \AA , respectively, which give a total current of 15 nA for a bias voltage of 1.8 V . As the

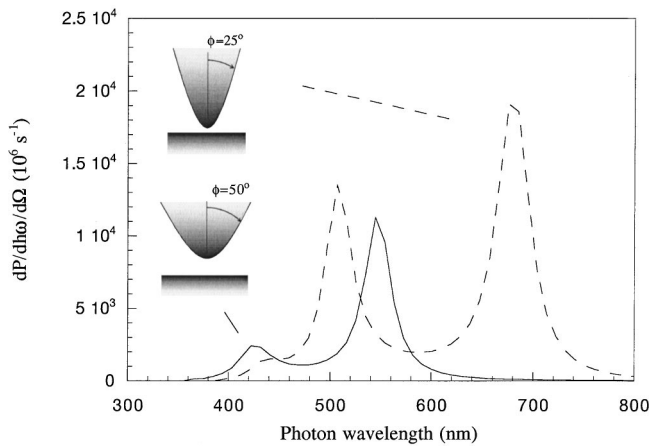


FIG. 8. Radiated power for two different silver tips on silver samples as a function of the wavelength of the emitted photons. The apertures ϕ used to characterize the tips are shown in the inset, and $b = 3.2 \text{ \AA}$ in both cases. The distance between the tip and sample is fixed in order to give a current of 10 nA when a 4-V bias is applied. Note how well this compares with the experimental spectra in Fig. 1.

aperture of the tip becomes smaller, the intensity of the emission slightly increases due to the shorter separation distance giving rise to a more effective coupling between the tip and sample. The smaller area of tunneling compensates for this tendency. A shift of 0.2 eV in the peak position is observed in the radiated power as a consequence of the different energies of the resonances for each cavity. Following the tendency pointed out in Sec. III, a tip with a small aperture shows a low-energy peak at 1.4 eV, whereas a tip with a larger aperture shows a peak at 1.6 eV. In both cases the peak corresponds to the same mode of the cavity which is shifted up as the shape changes. For a very narrow tip it may even be possible to detect higher-order peaks which actually appear in experimental situations for Au on Au (see Ref. 18). The intensity of both peaks is slightly different, since the two effects mentioned above (larger field enhancement and separation distance) do not cancel exactly. A similar tendency is also found for silver tips and samples. It is clear, therefore, that there is a general tendency for the strength of the emission peaks to show such a compensation when working at constant current, with an influence of the particular material which can slightly change this balance in one direction or the other.²⁹

In Fig. 8 the case of a silver tip and a silver sample is presented for the constant-current mode. The dashed line shows the case of a 25° tip aperture, whereas the solid line shows the case of a 50° tip aperture. Note the order of magnitude larger yield for Ag as compared to Au (Fig. 7). Two distinct peaks are found around 675 nm ($\sim 1.8 \text{ eV}$) and 500 nm ($\sim 2.45 \text{ eV}$) for the first case, which corresponds well to the positions found experimentally in Fig. 1. As the aperture becomes larger, the low-energy peak is shifted upward in

energy (down to 540 nm in wavelength), and so is the higher-order peak which almost disappears from the spectrum. In this sense, the detection of experimental peaks at different positions is most likely due to a shifting of modes depending on the aperture of the tip in use. In some cases this can shift them out of the spectrum range altogether. The mechanisms to explain the experimental peaks here are analogous to the ones presented for gold above, and are general features which can be used to estimate the tip aperture for any situation. It is interesting to point out here that low-energy peaks can also be reached in the emission spectrum by making the aperture larger, as is obvious in the mode distribution in Fig. 4, but this leads to unrealistic values of the tunneling distance. This fact makes sharp tips more plausible for describing different spectra, such as the ones in Fig. 1.

V. CONCLUSIONS

We have performed calculations of the light emission from metals surfaces in a scanning tunneling microscope. Compared to previous treatments, we have used a more flexible parametrization of the tip geometry, and a more accurate description of the tunneling current based on an extension of Tersoff and Hamann's theory, which also takes into account the geometry of the tip. In particular, the use of a hyperbolic tip shape enables a separate variation of the very apex of the tip and the aperture of the tip on a larger scale. This appears to be a more realistic description of experimental tips, which are believed to often be comprised of a shaft on a length scale governing the electromagnetic properties and a microtip supporting the tunneling current. We find that the tip aperture has a large impact on the position of peaks in the emission spectra, while the very apex is more important for the intensity. An important difference with respect to previous models is that we find two regimes of aperture angles with similar mode energies. For $\phi > 45^\circ$, the interaction of surface charges on the tip and sample dominates, but for $\phi < 45^\circ$ the interaction of surface charges on the faces of the tip itself dominates the physics. Moreover, in the latter case, the spatial extent of the tip-induced modes is found to be much smaller than expected on the basis of previous modeling for a spherical tip. It may be that this unexpected localization to a near-atomic scale has already been observed in experiments, where atomic resolution in photon mapping was achieved.²⁸ In future work, it may be possible to extend the model to include density-of-states effects of non-free-electron nature. Moreover, it will be interesting to study what happens when relaxing the rotational symmetry of the tip.

ACKNOWLEDGMENTS

We acknowledge stimulating discussions with P. Johansson, D. Penn, and R. Coratger. This work was carried out with financial support from the TMR network EMIT (Contract No. ERB-FMRX-CT98-0198), the Swedish Natural Science Research Council, and Iberdrola S.A.

*E-mail: aizpurua@fy.chalmers.se

¹J. K. Gimzewski, B. Reihl, J. H. Coombs, and R. R. Schlittler, *Z. Phys. B: Condens. Matter* **72**, 497 (1988).

²D. L. Abraham, A. Veider, Ch. Schönenberger, H. P. Meier, D. J.

Arent, and S. F. Alvarado, *Appl. Phys. Lett.* **56**, 1564 (1990).

³R. Berndt, R. Gaisch, J. K. Gimzewski, B. Reihl, R. R. Schlittler, W. D. Schneider, and M. Tschudy, *Science* **262**, 1425 (1993).

⁴D. T. Pierce, A. Davies, J. A. Stroscio, and R. J. Celotta, *Appl.*

- Phys. A: Mater. Sci. Process. **66**, S403 (1998).
- ⁵Y. Uehara, T. Fujita, and S. Ushioda, Phys. Rev. Lett. **83**, 2445 (1999).
- ⁶P. Johansson, R. Monreal, and P. Apell, Phys. Rev. B **42**, 9210 (1990).
- ⁷R. Berndt, J. K. Gimzewski, and P. Johansson, Phys. Rev. Lett. **67**, 3796 (1991); **71**, 3493 (1993).
- ⁸B. N. J. Persson and A. Baratoff, Phys. Rev. Lett. **68**, 3224 (1992).
- ⁹M. Tsukada, T. Schimizu, and K. Kobayashi, Ultramicroscopy **42-44**, 360 (1992).
- ¹⁰R. Berndt and J. K. Gimzewski, Phys. Rev. B **48**, 4746 (1993).
- ¹¹R. W. Rendell and D. J. Scalapino, Phys. Rev. B **24**, 3276 (1981).
- ¹²P. Johansson and R. Monreal, Z. Phys. B: Condens. Matter **84**, 269 (1991).
- ¹³A. Downes, M. E. Taylor, and M. E. Welland, Phys. Rev. B **57**, 6706 (1998).
- ¹⁴A. Madrazo, M. Nieto-Vesperinas, and N. García, Phys. Rev. B **53**, 3654 (1996).
- ¹⁵P. Johansson, Phys. Rev. B **58**, 10 823 (1998).
- ¹⁶L. Olsson, N. Lin, V. Yakimov, and R. Erlandsson, J. Appl. Phys. **84**, 4060 (1998).
- ¹⁷P. Johansson and P. Apell, Phys. Rev. B **56**, 4159 (1997).
- ¹⁸R. Péchou, R. Coratger, C. Girardin, F. Ajustron, and J. Beauvilain, J. Phys. III **6**, 1441 (1996).
- ¹⁹C. A. Brebbia, J. C. Telles, and L. C. Wrobel, *Boundary Element Techniques* (Springer, Berlin, 1984).
- ²⁰F. Ouyang and M. Isaacson, Philos. Mag. B **60**, 481 (1989).
- ²¹F. J. García de Abajo and J. Aizpurua, Phys. Rev. B **56**, 15 873 (1997).
- ²²L. D. Landau, E. M. Lifshitz, and L. P. Pitaevskii, *Electrodynamics of Continuous Media*, 2nd ed. (Pergamon, Oxford, 1984), pp. 308 and 309.
- ²³T. L. Ferrell, Nucl. Instrum. Methods Phys. Res. B **96**, 483 (1995).
- ²⁴W. Heitler, *The Quantum Theory of Radiation*, 3rd ed. (Dover, New York, 1984), Chap. IV, p. 16.
- ²⁵J. Bardeen, Phys. Rev. Lett. **6**, 57 (1961).
- ²⁶J. Tersoff and D. R. Hamann, Phys. Rev. B **31**, 805 (1985).
- ²⁷K. Stokbro, U. Quaade, and F. Grey, Appl. Phys. A: Mater. Sci. Process. **66**, S907 (1998).
- ²⁸R. Berndt, R. Gaisch, W.-D. Schneider, J. K. Gimzewski, B. Reihl, R. R. Schlittler, and M. Tschudy, Phys. Rev. Lett. **74**, 102 (1995).
- ²⁹S. P. Apell, P. M. Echenique, and R. H. Ritchie, Ultramicroscopy **65**, 53 (1996).